# Negative Charges in the Transmembrane Domains of the HERG K Channel Are Involved in the Activation- and Deactivation-gating Processes

Jie Liu, Mei Zhang, Min Jiang, and Gea-Ny Tseng

Department of Physiology, Virginia Commonwealth University, Richmond, VA 23298

ABSTRACT  The transmembrane domains of HERG (S1–S3) contain six negative charges: three are conserved in all voltage-gated K channels (D456 and D466 in S2, D501 in S3) and three are unique to the EAG family (D411 in S1, D460 in S2, and D509 in S3). We infer the functional role of these aspartates by studying how substituting them with cysteine, one at a time, affects the channel function. D456C is not functional, suggesting that this negative charge may play a critical role in channel protein folding during biogenesis, as has been shown for its counterpart in the Shaker channel. Data from the other five functional mutants suggest that D411 can stabilize the HERG channel in the closed state, while D460 and D509 have the opposite effect. D466 and D501 both may contribute to voltage-sensing during the activation process. On the other hand, all five aspartates work in a concerted fashion in contributing to the slow deactivation process of the HERG channel. Accessibility tests of the introduced thiol groups to extracellular MTS reagents indicate that water-filled crevices penetrate deep into the HERG protein core, reaching the cytoplasmic halves of S1 and S2. At these deep locations, accessibility of 411C and 466C to the extracellular aqueous phase is voltage dependent, suggesting that conformational changes occur in S1 and S2 or the surrounding crevices during gating. Increasing extracellular $[H^+]$ accelerates HERG deactivation. This effect is suppressed by substituting the aspartates with cysteine, suggesting that protonation of these aspartates may contribute to the signaling pathway whereby external $[H^+]$ influences conformational changes in the channel's cytoplasmic domains (where deactivation takes place). There is no evidence for a metal ion binding site coordinated by negative charges in the transmembrane domains of HERG, as the one described for the EAG channel.

KEY WORDS:   mutagenesis • *Xenopus* oocytes • structure-function relationship • voltage-gated K channel

## INTRODUCTION

HERG is encoded by the human ether-a-go-go–related gene (HERG)* and functions as the pore-forming component of the rapid delayed rectifier K ($I_{Kr}$) channel in the heart (Sanguinetti et al., 1995). The focus of this study is the negatively charged residues in the transmembrane domains (S1, S2 and S3) of HERG. Fig. 1 A shows an alignment of amino acid sequences of these domains, along with those of S4, for HERG and two voltage-gated K (Kv) channels (EAG and Shaker), for which the functional roles of the negative charges in the transmembrane domains have been studied (Papazian et al., 2002). There are 3 negative charges well conserved in all Kv channels known so far (Papazian et al., 2002). They are denoted as −2, −4, and −5 in Fig. 1. The functional role for these conserved negative charges in the Shaker channel has been thoroughly studied by Papazian and her colleagues (Seoh et al.,

1996; Tiwari-Woodruff et al., 1997, 2000; Papazian et al., 2002). E283 (−2) can form a specific salt-bridge with R368 (+3) or R371 (+4) in the S4 domain during biogenesis. This helps ensure a proper folding of the Shaker channel protein, which can mature and reach the cell surface (Tiwari-Woodruff et al., 1997). Once the channel is in the cell-surface membrane, these negative charges engage in the gating processes in several ways. They may face water-filled crevices that penetrate into the protein core. By shaping the local electrical field in the crevices surrounding the major voltage sensor, S4, these negative charges can indirectly affect the channel's gating process (Islas and Sigworth, 2001). E283 may facilitate channel activation by forming a salt-bridge with R368 in an intermediate state during activation transitions, and with R371 when the channel reaches the final open state, thus stabilizing the channel in the activated states (Seoh et al., 1996; Tiwari-Woodruff et al., 2000). E293 may move relative to the membrane electrical field during gating, thereby directly contributing to the channel's gating charge (Seoh et al., 1996).

The EAG channel has more negative charges in the transmembrane domains (Papazian et al., 2002, Silverman et al., 2000). They are marked by −1, −3, and −6

Gea-Ny Tseng, Department of Physiology, Virginia Commonwealth University, 1101 E. Marshall Street Richmond, VA 23298. Fax: (804) 828-7382; E-mail: gtseng@hsc.vcu.edu

*Abbreviations used in this paper:* HERG, human ether-a-go-go–related gene; MTS, methanethiosulfonate.
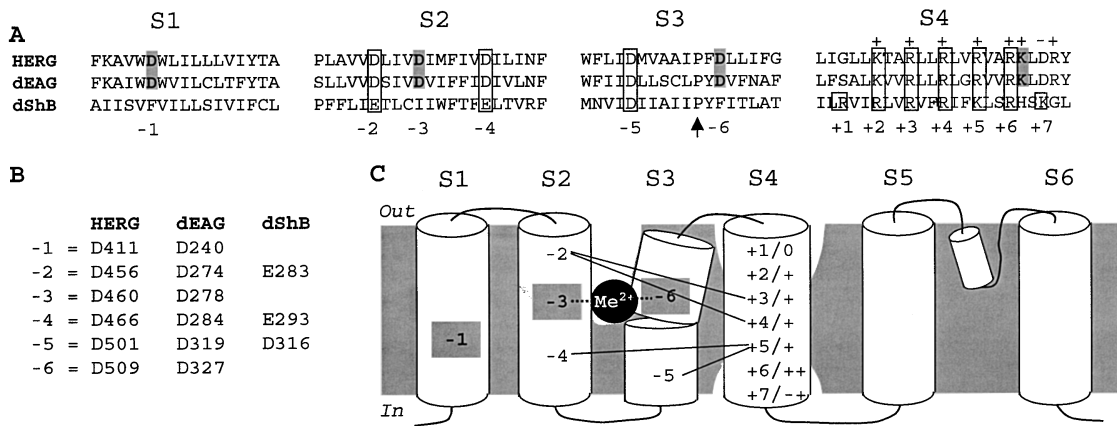
**A**

|  | S1 | S2 | S3 | S4 |
|---|---|---|---|---|
| **HERG** | FKAVVDWLILLLVIYTA | PLAVVDLIVDIMFIVDILINF | WFLIDMVAAIPFDLLIFG | LIGLLKTARLLRLVRVARKLDRY |
| **dEAG** | FKAIWDWVILCLTFYTA | SLLVVDSIVDVIFFIDIVLNF | WFIIDLLSCLPYDVFNAF | LFSALKVVRLLRLGRVVRKLDRY |
| **dShB** | AIISVFVILLSIVIFCL | PFFLIETLCIIWFTFELTVRF | MNVIDIIAIIPYFITLAT | ILRVIRLVRVFRIFKLSRHSKGL |

-1 (S1)   -2  -3  -4 (S2)   -5  ↑ -6 (S3)   + + + + + ++ -+   +1 +2 +3 +4 +5 +6 +7 (S4)

**B**

| | HERG | dEAG | dShB |
|---|---|---|---|
| -1 = | D411 | D240 | |
| -2 = | D456 | D274 | E283 |
| -3 = | D460 | D278 | |
| -4 = | D466 | D284 | E293 |
| -5 = | D501 | D319 | D316 |
| -6 = | D509 | D327 | |

**C**   S1   S2   S3   S4   S5   S6

Out / In   -2  -3  -6  Me$^{2+}$  -4  -5   +1/0  +2/+  +3/+  +4/+  +5/+  +6/++  +7/-+   -1

FIGURE 1. (A) Alignment of amino acid sequences of S1–S4 transmembrane domains for HERG, *Drosophila* EAG (dEAG), and Shaker (dShB). The S1–S3 alignments are based on the conserved aspartate or glutamate residues (D and E, highlighted by gray shades or boxes). The S4 alignment is that proposed in Gandhi and Isacoff (2002), which is based on the state dependence of side chain accessibility to extracellular MTS reagents. The negatively charged residues in S1–S3 are designated as −1 to −6. The positive charges in dShB S4 are designated as +1 to +7. The charge distribution along S4 in HERG and dEAG differs from that of dShB, as is noted above the amino acid sequences. The arrow points to well-conserved proline residues that cause a kink in the S3 helix (Li-Smerin and Swartz, 2001). (B) Residues and position numbers for the negatively charged residues in S1–S3 of HERG and dEAG, and S2–S3 of dShB. (C) Cartoon of transmembrane topology of a Kv channel subunit, highlighting: (a) the negative and positive charges in the transmembrane domains, (b) difference in S4 charge distribution between dShB and HERG or dEAG, (c) known interactions between charged residues in dShB (−2 with +3 and +4, −4, and −5 with +5; Papazian et al., 2002), (d) a metal ion (Me$^{2+}$) binding site formed by −3 and −6 in dEAG (Papazian et al., 2002), and (5) putative water-filled crevices around S2, S3, and S4 (in the activated state).

in Fig. 1. The EAG channel has a unique gating property among Kv channels: prepulse hyperpolarization can delay EAG activation not only by increasing the transition time among closed states ("Cole-Moore shift," as is generally observed for Kv channels; Cole and Moore, 1960), but also by slowing the final opening transition (Tang et al., 2000). Increasing the extracellular Mg$^{2+}$ concentration ([Mg$^{2+}$]$_o$) can accentuate the slowing effect of prepulse hyperpolarization (Terlau et al., 1996; Tang et al., 2000). It has been shown that negative charges −3 and −6 can coordinate a divalent cation binding site within the EAG channel (Silverman et al., 2000). It is further suggested that Mg$^{2+}$ binding to this cation-binding site limits S4's outward movement during membrane depolarization, thus slowing channel activation (Schonherr et al., 2002). Whether the negative charge in S1 (−1 in Fig. 1) plays any role in EAG channel function has not been examined.

As its name implies, HERG is related to the EAG channel (Warmke and Ganetzky, 1994). Despite the homology in amino acid sequence between HERG and EAG channels (e.g., Fig. 1 A), there are distinct differences in their gating behavior. The rate of HERG activation and deactivation is much slower than that of EAG. HERG has a uniquely strong and fast C-type inactivation process, while EAG inactivates to a much lesser degree and more slowly (Sanguinetti et al., 1995; Robertson et al., 1996; Herzberg et al., 1998). HERG shares the conserved as well as the extra negative charges in the transmembrane

domains (Fig. 1 A). What is the role of these negative charges in its function? Besides the question about whether −1 has any functional role, there are three more reasons to ask this question. First, extracellular acidosis (changing pH$_o$ from 7.5 to 6.5) has a selective effect on the rate of HERG deactivation (Jiang et al., 1999). The mechanism is not clear, because deactivation in the HERG channel, as in other Kv channels, is mediated by conformational changes in the cytoplasmic domains (S4-S5 linker and cytoplasmic half of S6) (Lu et al., 2002; Tristani-Firouzi et al., 2002). The slow rate of deactivation in the HERG channel is further due to an interaction between the NH$_2$-terminal "PAS" domain (aa 2–138) (Morais Cabral et al., 1998) and the S4-S5 linker (Wang et al., 1998), which stabilizes the channel in the open state. However, there is a strong possibility that extracellular acidosis may transmit the signal to cytoplasmic domains by protonating carboxylate side chains in the transmembrane domains of HERG. Second, the effects of extracellular Mg$^{2+}$ on HERG are distinctly different from those on the EAG channels (Ho et al., 1998; Tang et al., 2000). Elevating [Mg$^{2+}$]$_o$ in the range of 1–10 mM slows EAG activation without any effect on the voltage dependence of activation or the rate of deactivation (Tang et al., 2000). On the other hand, changing [Mg$^{2+}$]$_o$ in the same range causes a prominent positive shift in the voltage-dependent activation and a marked acceleration of deactivation in HERG (Ho et al., 1998). This raises the question as to whether Mg$^{2+}$ affects the HERG channel

by the same mechanism, i.e., binding to a metal ion binding site in the transmembrane domain, as has been described for the EAG channel. Third, the charge distribution along the S4 domain in HERG differs from that in the Shaker channel. According to the proposed S4 alignment (Gandhi and Isacoff, 2002), HERG lacks the first positive charge (+1) in S4. Furthermore, the charge distribution around the S4 surface after +5 in HERG is very different from that in Shaker. These differences may entail a pattern of interaction between the S4 and the negative charges in HERG different from that described for the Shaker channel (highlighted in Fig. 1 C).

We ask three questions in this study: (a) How does neutralizing the negative charges in S1–S3 of HERG affect the channel function? (b) Are these aspartate side chains accessible to the extracellular solution? (c) Are these negative charges involved in HERG channel modulation by extracellular $H^+$ and divalent cations? The answer to the second question bears on the answer to the third one. We choose to substitute these aspartate residues with cysteine. The side chain volume of cysteine is 108.5 $A^3$, not very different from that of aspartate side chain (111.1 $A^3$). More importantly, the cysteine side chain is highly reactive to methanethiosulfonate (MTS) reagents. This allows us to probe the side chain accessibility by applying membrane impermeable MTS reagents to the bath solution. These mutants are designated by D (for aspartate), position number, and C (for cysteine). Among the six mutants created, D456C (−2 in S2, Fig. 1) does not produce functional channels despite repeated attempts. This suggests that the negative charge at 456 may play a critical role in protein folding during biogenesis of the HERG channel (Tiwari-Woodruff et al., 1997). This mutant is not included in the current study.

MATERIALS AND METHODS

*Mutagenesis*

HERG in a vector, pGH19 (a gift from Dr. Gail A. Robertson, University of Wisconsin-Madison), was subcloned into the KpnI-XbaI site of pAlterMax. Mutagenesis was performed using the oligonucleotide-directed method and a commercial kit (Alter site II in vitro Mutagenesis System; Promega). Mutations were confirmed by direct DNA sequencing around the mutation sites. Two independent colonies were picked and used for cRNA transcription and oocyte expression. No differences in the channel phenotype were noticed between two colonies from the same mutant. For transcription, plasmids were linearized by NotI and transcribed using T7 RNA polymerase using a commercial kit (Mmessage Mmachine; Ambion). The quality and quantity of cRNA products were evaluated using densitometry (ChemiImager model 4400; α-Innotech Corp).

*Oocyte Preparation*

Oocytes were isolated as described before (Tseng-Crank et al., 1990), incubated in an ND96-based medium (composition given below), and supplemented with 10% horse serum and penicil-

lin/streptomycin) at 16°C. 5–12 h after isolation, each oocyte was injected with 40 nl of cRNA solution (containing cRNA of 4–18 ng), using a Drummond digital microdispenser. Oocytes were incubated in the above medium at 16°C, and studied 2–4 d after cRNA injection.

*Voltage Clamp Experiments*

Before recording, oocytes expressing cysteine-substituted mutants were pretreated with DTT: incubation in freshly made DTT solution (5 mM in the incubation medium described above) at room temperature for 2–4 h, followed by three washes in 3 ml of DTT-free incubation medium. Membrane currents were recorded from whole oocytes using the "2-cushion pipette" voltage clamp method (Schreibmayer et al., 1994). Both current-passing and voltage-recording pipettes had tip resistance 0.1–0.3 MΩ. During recordings, the oocyte was continuously superfused with a low-Cl ND96 solution to reduce interference from endogenous Cl channels. Voltage clamp was done at room temperature (24–26°C) with OC-725B or OC-725C amplifier (Warner Instruments). Voltage clamp protocol generation and data acquisition were controlled by pClamp5.5 via a 12-bit D/A and A/D converter (DMA, Axon Instruments, Inc.). Current data were low-pass filtered at 1 kHz (Frequency Devices) and stored on disks for off-line analysis.

*Voltage Clamp Protocols and Data Analysis*

To study voltage dependence of activation, the following protocol is used: from $V_h$ −80 mV, 1-s test pulses to $V_t$ ranging from −70 to +60–120 mV (depending on the voltage range of channel activation) in 10-mV increments are applied once every 15 s. The peak amplitudes of tail currents are normalized by the maximal tail current following $V_t$ to +60 mV. This gives an estimate of the "fraction of channels activated" at the end of the 1-s test pulses. Its voltage dependence is analyzed by fitting the data with a simple Boltzmann function:

$$\text{fraction activated} = 1/\{1 + \exp[z_g(V_{0.5} - V_t)F/RT]\}, \quad (1)$$

where $V_{0.5}$ and $z_g$ are the half-maximum activation voltage and apparent gating charge, respectively, F is Faraday constant, R is gas constant, and T is absolute temperature (F/RT = 0.04 $mV^{-1}$). The same protocol and data analysis are applied to all functional mutant channels except D411C. The activation curve of D411C requires an empirical double Boltzmann function for a good fit:

$$\text{fraction activated} = A_1/\{1 + \exp[z_1(V_1 - V_t)F/RT]\} \quad (2)$$
$$+ A_2/\{1 + \exp[z_2(V_2 - V_t)F/RT]\},$$

where $A_i$, $V_i$, and $z_i$ are the fraction, half-maximum activation voltage, and apparent gating charge for the *i*th Boltzmann component.

The time constant of activation ($\tau_o$) and its voltage dependence are studied using an "envelope test" protocol: from $V_h$ −80 mV, test pulses to $V_t$ ranging from −20 to 60 mV in 20-mV increments for varying durations are applied once every 15 s. The time course of growth of peak tail current amplitude can be well fit with a single exponential function with a time delay:

$$I_{tail} = I_{max} \times \{1 - \exp[-(t - t_{delay})/\tau_o]\}, \quad (3)$$

where $I_{tail}$, $I_{max}$, t, $t_{delay}$, and $\tau_o$ are the peak tail current amplitude after a test pulse of duration t, the asymptotic value of $I_{tail}$, test

pulse duration, time delay, and $\tau$ of activation, respectively. To estimate the voltage dependence of the opening transition, the following equation is used ($K_o$ is the reciprocal of $\tau_o$, see Scheme I in RESULTS):

$$K_o(V) \;=\; K_o(0) \times \exp(z_a VF/RT), \qquad (4)$$

where $K_o(V)$ and $K_o(0)$ are rate constants of channel opening at test pulse voltages of V and 0 mV, respectively, and $z_a$ is the apparent gating charge for channel opening. The value of $z_a$ is obtained by a linear regression analysis of relationship between $\ln(K_o(V))$ and $V_t$ in an appropriate $V_t$ range (e.g., $-40$ to 40 mV for WT in Fig. 2 B). Since channels need to make transitions between closed states before opening, $1/\tau_o$ does not approximate $K_o$ until the voltage is positive enough so that the degree of activation has plateaued. In Fig. 2 B, the voltage dependence of $\tau_o$ appears to decrease in this voltage range, suggesting that $K_o$ is not very voltage dependent and that our fit of the data overestimates the charge associated with the opening transition. Therefore, $z_a$ probably reflects the charge associated with closed state transitions.

To construct the fully activated current-voltage ($I_{f\text{-}a}$-V) relationship, the following protocol is used: from $V_h$ $-80$ mV, 0.2-s conditioning pulses to $+60$ mV are applied to fully activate the channels once every 15 s, followed by repolarization to $V_r$ $+30$ to $-120$ mV in 10-mV increments. The peak tail current amplitudes are normalized by the maximum outward tail current at $V_r$ $-50$ or $-60$ mV, and averaged over cells.

To estimate the time constant of the major (fast) component of deactivation ($\tau_c$) in the voltage range below the threshold of channel activation, a voltage clamp protocol similar to that used to construct the $I_{f\text{-}a}$-V relationship is used. Time course of decay of tail current in a voltage range negative to the activation threshold is fit with a double-exponential function:

$$I_{tail}(t) \;=\; I_{Fast} \times \exp(-t/\tau_{Fast}) + I_{Slow} \times \exp(-t/\tau_{Slow}) + I_{SS}, \quad (5)$$

where $I_{tail}(t)$ is tail current amplitude at time t after the beginning of repolarization, $I_{Fast}$, $I_{Slow}$, and $I_{SS}$ are the fast, slow, and steady-state components of tail current, $\tau_{Fast}$ ($= \tau_c$) and $\tau_{Slow}$ are time constants of the two time-dependent current component.

To study the rate of C-type inactivation in HERG and its mutants, a three-pulse voltage clamp protocol is used: from $V_h$ $-80$ mV, depolarization to $+40$ mV for 1 s is applied to activate then inactivate the channels. This is followed by a 10-ms step to $-80$ mV, during which channels recover from inactivation without appreciable deactivation. Then a third pulse to $V_3$ ranging from $+40$ to $-20$ mV is applied during which the channels (recovered from inactivation and still in the activated state) reinactivate. The decay phase of current during $V_3$ (excluding the capacitive transient during the first 2 ms) can be well fit with a single exponential function, which allows the determination of time constant of inactivation ($\tau_I$).

To study the voltage dependence of accessibility of introduced cysteine side chains to extracellular MTSET, the following general voltage clamp protocol is used: currents are elicited by repetitive 1-s pulses from $V_h$ $-80$ to $+20$ mV once every 30 s. Three pulses are applied before MTSET to confirm current stability (pulses 1–3). Then the membrane voltage is held at $V_h$ of either $-80$, $-20$, or $+20$ mV for 10 min, during which the oocyte is superfused with MTSET solution (1 mM) for 5 min, followed by a 5-min wash. Four or more pulses are then resumed to test for MTSET effects (pulses 4–7).

In the voltage clamp protocols described for the construction of activation curve and $I_{f\text{-}a}$-V relationship, a 10-ms prepulse from $V_h$ $-80$ mV to $-100$ mV precedes every depolarization pulse. Currents jump during these prepulse is used for leak-subtraction. The following software is used for data analysis: pClamp6 or 8, EXCEL (Microsoft), SigmaPlot, SigmaStat, and PeakFit (SPSS).

*Cysteine Side Chain Modification*

MTSET or MTSES (Toronto Research Chemicals, Inc.) powder was dissolved in deionized water at 0.1 M shortly before experiments. The stock solution was stored on ice and used within 2 h After control data were obtained, the MTSET or MTSES stock solution was diluted with bath solution to 1 or 10 mM and applied to the oocyte immediately.

*Solutions*

The ND96 solution had the following composition (in mM): NaCl 96, KCl 2, $CaCl_2$ 1.8, $MgCl_2$ 1, HEPES 5, Na-pyruvate 2.5, pH 7.5. The low-Cl ND96 used during voltage clamp experiments were made with $Cl^-$ ions in ND96 replaced by methanesulfonate. In some experiments, [K] in low-Cl ND96 was raised to 98 mM. In this case, $Na^+$ and Na-pyruvate were omitted to maintain the osmolality. Solutions with pH 6.5 and 8.5 were titrated with methanesulfonic acid or NaOH to the desired pH. Solution of 10 mM $[Ca^{2+}]$ was made by adding $CaCl_2$ without compensation for osmolality.

RESULTS

We replace aspartate residues in S1, S2, and S3 of HERG (D411, D456, D460, D466, D501, and D509, Fig. 1) by cysteine, one at a time. The mutants produce functional channels except D456C. For the functional mutants, we study the effects of cysteine substitution on the channel function, accessibility of the introduced thiol side chains to extracellular hydrophilic MTS reagents, and the effects of mutations on channel modulation by extracellular $H^+$ and $Ca^{2+}$ ions. The voltage clamp protocols and methods of data analysis used to characterize channel function are illustrated in Fig. 2, using wild-type (WT) HERG as an example. The voltage dependence of activation is characterized by a "1-s isochronal" activation curve (Fig. 2 A), which can be well fit with a simple Boltzmann function for WT and mutant channels except D411C (Fig. 3 B). We use two parameters generated from curve fitting (half-maximum activation voltage, $V_{0.5}$, and apparent gating charge for channel activation, $z_g$) to compare the voltage dependencies of channel activation.

The rate of activation is measured using an "envelope test" protocol (Fig. 2 B). Because the C-type inactivation in the HERG channel is extremely fast relative to channel activation, the activation rate cannot be directly measured from the time course of current during depolarization. On the other hand, upon repolarization the channels rapidly recover from C-type inactivation before deactivation sets in. Therefore, the growth of peak tail current amplitude after increasing durations of depolarization can be used to trace the time course of channel activation. This time course can be well described by a single exponential function with a
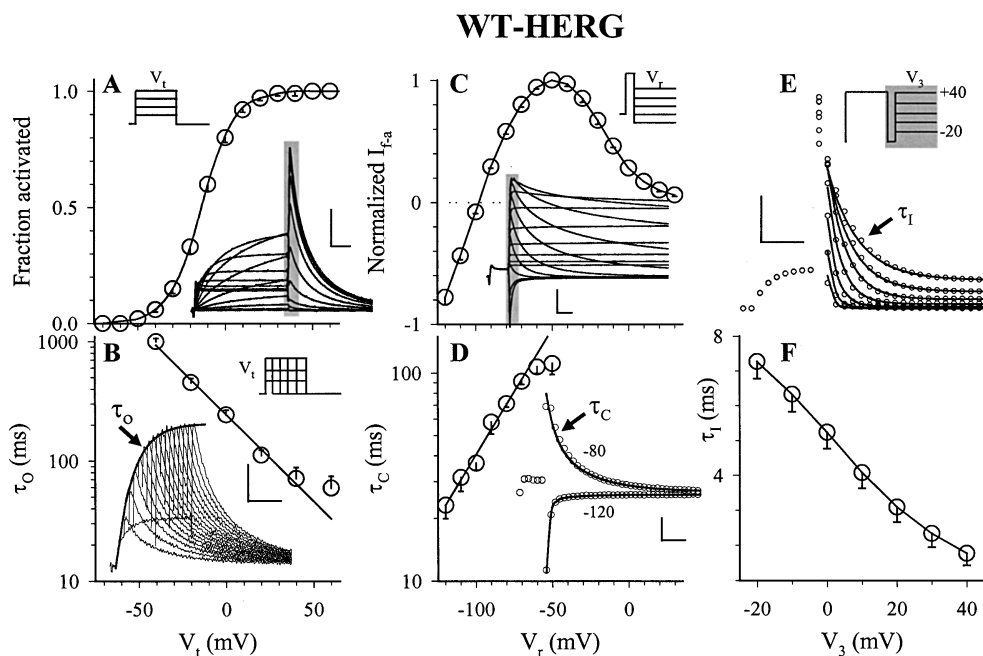
## WT-HERG



FIGURE 2. Voltage clamp protocols and data analysis for the characterization of channel function using wild-type (WT) HERG as an example. (A) Voltage dependence of activation. Top inset: voltage clamp protocol. Bottom inset: representative original current traces elicited by the protocol. The gray shade highlights the peak of tail currents that is used to estimate the degree of channel activation. The main graph depicts summary activation curve calculated from Eq. 1, $V_{0.5} = -13.6 \pm 1.3$ mV and $z_g = 2.70 \pm 0.07$. (B) Time constant of activation ($\tau_o$) and its voltage dependence. Top inset: "envelope test" protocol. Bottom inset: representative original current traces elicited by the envelope test protocol at a $V_t$ of +20 mV. The solid curve superimposed on the current traces is calculated from Eq. 3, with $t_{delay} = 1.7$ ms and $\tau_o = 97$ ms. The main graph depicts summary data plotted on a semilogarithmic scale, superimposed on a line calculated from Eq. 4. The value of $z_o$ is obtained by a linear regression analysis of relationship between $\ln(K_o(V))$ and $V_t$ in the $V_t$ range of $-40$ to $+40$ mV (0.83). (C) Fully-activated current-voltage ($I_{f-a}$-V) relationship. Top inset: voltage clamp protocol. Bottom inset: original current traces elicited by the protocol. The gray shade highlights the peak tail current amplitudes used to construct the $I_{f-a}$-V curve. The main graph depicts the average $I_{f-a}$-V relationship. (D) Time constant of the fast component of deactivation. The protocol is the same as that in C. Inset: original data (open circles, showing only every twentieth data points) and fitting result (superimposed solid curves) at $V_r$ $-80$ and $-120$ mV. The main graph reports $\tau_c$ values plotted on a semilogarithmic scale. (E) Voltage clamp protocol and curve fitting to estimate the time constant of inactivation ($\tau_I$). The main graph depicts current traces (plotted every twentieth data points) recorded during the second and third pulses (shaded portion of the protocol), superimposed with one-exponential fit to the decay phase during the third pulse. (F) Summary data of $\tau_I$ values from $-20$ to $+40$ mV. Data shown in the main graphs are summarized from 3–11 cells each. These WT data are shown again as open triangles in Figs. 3–6 and 8, as a comparison with data from mutant channels. Calibration bars correspond to 1 µA and 0.2 s, except those in E (5 µA and 10 ms).

short delay (Fig. 2 B, inset, and Eq. 3 in MATERIALS AND METHODS). The time delay (to account for the initial sigmoidal phase of current activation) is much shorter than the single exponential rising component (Fig. 2 B, legend). This suggests that the channel spends relatively little time in transitions among closed states ($C_0$ to $C_{n-1}$, Scheme I), but more time in the final opening step ($C_n$ to $O$):

relatively fast transitions        $K_o(V)$
$(C_0 \rightarrow C_1 \rightarrow C_2 \ldots C_{n-1}) \rightarrow C_n \xrightarrow{} O$
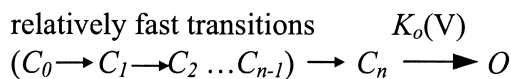
SCHEME I

where $K_o(V)$ is the rate constant of transition from $C_n$ to $O$ at voltage V. Note that the inactivated state is omitted in this simplified gating scheme. This is justified because the envelope test protocol negates influence from channel inactivation on the measurement. $K_o(V)$ is estimated by the reciprocal of $\tau_o(V)$, the time constant of activation at voltage V, obtained by curve fitting. The relationship between $\tau_o(V)$ and depolarization voltage ($V_t$) is plotted on a semilogarithmic scale

in Fig. 2 B. It is clear that this relationship is largely linear over the $V_t$ range of $-40$ to $+40$ mV. The exponential relationship between $\tau_o(V)$ and $V_t$ indicates a voltage-dependent opening transition, thus:

$$K_o(V) = K_o(V)\exp(z_a VF/RT), \qquad (6)$$

where $K_o(0)$ is the rate constant of opening transition at 0 mV, and $z_a$ is the apparent gating charge involved in channel opening. A linear regression analysis on data shown in Fig. 2 B gives an estimate of $K_o(0)$ and $z_o$ of 1.4 $s^{-1}$ and 0.83 for the WT HERG.

The fully activated current-voltage ($I_{f-a}$-V) relationship as shown in Fig. 2 C can be used to deduce the pore-domain function: $K^+$ selectivity and C-type inactivation (Liu et al., 2002). The reversal potential ($E_{rev}$) of the $I_{f-a}$-V relationship for WT HERG is $-102.2 \pm 0.7$mV. This is very close to the estimated $E_K$ ($-105$ mV), suggesting a strong $K^+$ selectivity. The negative slope of the $I_{f-a}$-V relationship between $-60$ and $+30$ mV reflects a decrease in channel conductance due to C-type inacti-

vation. The kinetics of C-type inactivation is further analyzed by the three-pulse protocol (Fig. 2 E) and the summary data are presented in Fig. 2 F.

The time course of HERG deactivation can be well described by a double-exponential function. The fast phase of deactivation is the major component in the voltage range negative to the threshold of channel activation (accounting for ∼60% of the tail current at $V_r$ −80 mV, and ∼100% at −100 mV and more negative $V_r$). Therefore, we used these time constants to compare the rate of channel closing in the negative voltage range (Fig. 2 D).

Voltage clamp protocols and data analysis similar to those described for WT HERG are used to characterize the mutant channels' function. Where modifications are necessary, due to mutation-induced alterations in voltage dependence and/or kinetics of gating, they are specified in the figures. For a clear comparison, the WT data in Fig. 2 are shown again in the following figures reporting mutant channels' function.

### Effects of Replacing Aspartates in HERG's Transmembrane Domains with Cysteine on the Channel Function

*D411C in the intracellular half of S1 domain.* The gating behavior of D411C differs from that of WT HERG in three aspects. First, the voltage dependence of D411C activation manifests two apparent Boltzmann components, with ∼50% of the channels activated in a more negative voltage range than that of the WT channels, while the remaining 50% superimposed with the WT activation curve at voltages > 0 mV (Fig. 3 B). Second, the rate of D411C activation is much faster than that of WT. This is indicated by the early peak outward current followed by a decay in the D411C current traces during membrane depolarization (Fig. 3 A, but more clearly seen in Fig. 3 C, inset). The decay phase is due to the same fast C-type inactivation process as in the WT channel (Fig. 3 D). Since the rate of D411C activation becomes much faster, a large part of the C-type inactivation process occurs after channel activation, creating the early peak followed by a decay phase. Upon membrane repolarization, D411C quickly recovers from this C-type inactivation, as is the case for the WT channel. Therefore, the envelope test can be used to deduce the time course of D411C activation (Fig. 3 C, inset). For D411C, the $\tau_o$ values are shorter than those of WT in the voltage range of −20 to +40 mV, and the voltage sensitivity is modestly reduced ($z_o = 0.47$). Third, the rate of D411C deactivation is much faster than that of WT (Fig. 3 E). D411C is similar to WT in having a prominent and fast C-type inactivation process and a strong $K^+$ selectivity (Fig. 3 D).

*D460C in the middle of S2 domain.* Fig. 4 shows that the gating behavior of D460C differs from that of WT HERG in three aspects. First, the activation curve of
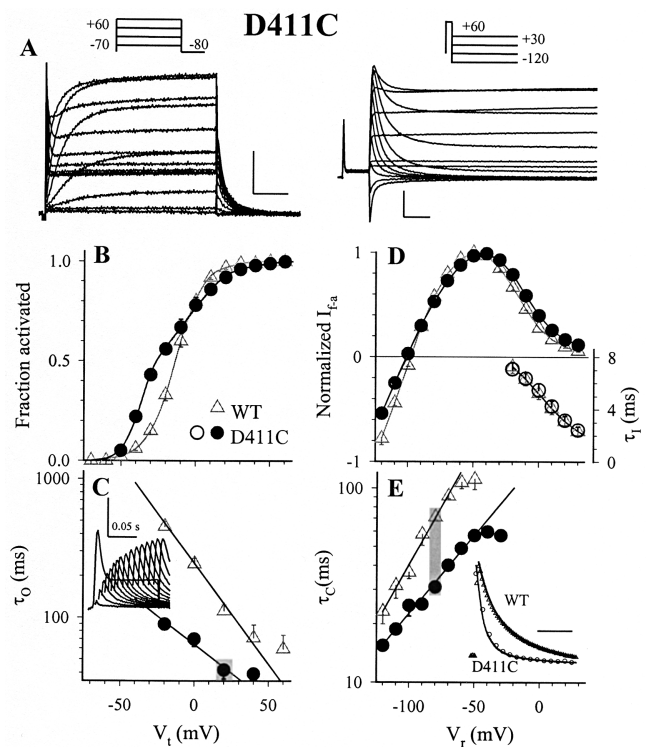


FIGURE 3. D411C channel function. (A) Representative D411C current traces elicited by the voltage clamp protocols shown on top. (B) Comparison of activation curve of D411C with that of WT-HERG. D411C and WT data are shown as closed circles and open triangles, respectively (same for C–E except $\tau_I$ values in D, for which D411C data are depicted as open circles). The curve superimposed on the D411C data points is calculated from Eq. 2 with: $A_1 = 0.47 \pm 0.03$, $V_1 = -37.6 \pm 0.9$ mV, $z_1 = 4.83 \pm 0.42$, $A_2 = 0.53 \pm 0.03$, $V_2 = -3.7 \pm 2.4$ mV, and $z_2 = 2.06 \pm 0.16$. (C) Comparison of $\tau$ of activation between D411C and WT. (Inset) D411C current traces elicited by the envelope test protocol at $V_t$ +20 mV. (Main graph) D411C data points are superimposed on a line calculated from Eq. 4, with $z_o = 0.47$. (D) Comparison of $I_{F-a}$-V relationship (left ordinate) and $\tau_I$ values (right lower ordinate) between D411C and WT. (E) Comparison of $\tau_c$ of deactivation between D411C and WT. (Inset) Superimposed D411C and WT tail currents recorded at $V_r$ −80 mV, with open symbols showing every twentieth data point and solid curves showing calculations from Eq. 5. The current amplitudes are scaled to match the peaks. (Main graph) Summary of D411C data versus WT data. D411C data in main graphs are averaged from 5 to 10 cells each. The gray shade in C and E indicates the voltages at which the original current traces shown in insets are measured. Calibration bars correspond to 1 μA and 0.2 s (except panel C inset, for which the time calibration bar is 50 ms).

D460C is shifted in the positive direction in a parallel fashion (Fig. 4 B). Second, the rate of D460C activation is slower than that of WT, although the voltage sensitivity is similar (Fig. 4 C). Third, the rate of D460C deactivation is much faster than that of WT (Fig. 4 E). D460C manifests a fast C-type inactivation process and a strong $K^+$ selectivity similar to those of WT HERG (Fig. 4 D).
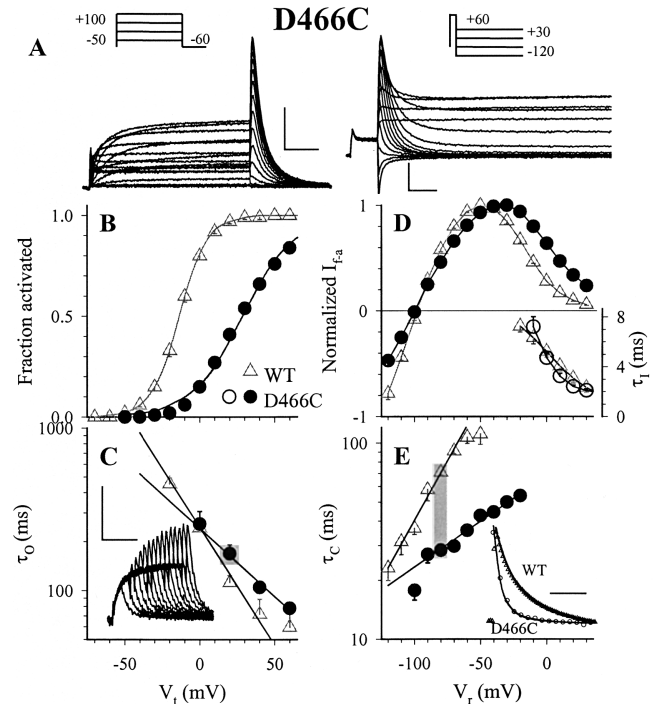
*D466C in the intracellular half of S2 domain.* Fig. 5 B shows that relative to the WT channel, the voltage de-
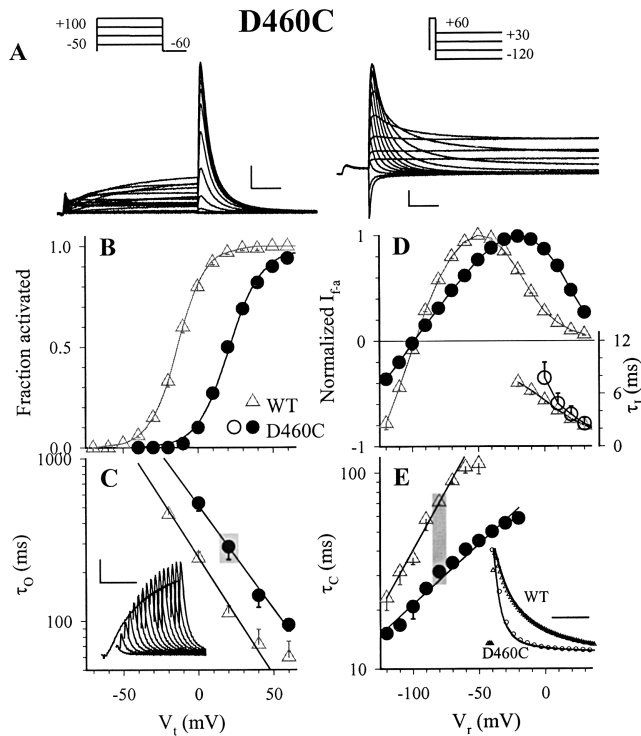
FIGURE 4. D460C channel function. The format of this figure is the same as that of Fig. 3. The D460C data in main graphs are averaged from seven to nine cells each. In B, the D460C activation curve has $V_{0.5} = 20.9 \pm 0.3$ mV, and $z_g = 2.35 \pm 0.08$. In C, D460C data points are superimposed on a line calculated from Eq. 4 with $z_o = 0.83$. Calibration bars correspond to 1 μA and 0.2 s.

FIGURE 5. D466C channel function. The format is the same as that of Fig. 3. D466C data in main graphs have $n = 5–11$ each. In B, the D466C activation curve has $V_{0.5} = 28.2 \pm 0.9$ mV, and $z_g = 1.48 \pm 0.01$. In C, the D466C data points are superimposed on a line calculated from Eq. 4 with $z_o = 0.48$. Calibration bars correspond to 1 μA and 0.2 s.

pendence of D466C activation is shifted in the positive direction. Furthermore, the rate of D466V activation is slower than that of WT in the $V_t$ range $> 0$ mV (Fig. 5 C), and the rate of D466C deactivation is faster than that of WT (Fig. 5 E). These changes are similar to those described for D460C. However, the effect of mutation on the voltage dependence of activation differs between the two. The voltage dependence is not altered by D460C. On the other hand, in D466C the voltage sensitivity of activation gating is reduced: the $z_g$ value is reduced to 1.48 (from 2.70 in WT), and the $z_a$ value is reduced to 0.48 (from 0.83 in WT). Despite the decrease in $z_a$, the $K_o(0)$ value is the same as that of WT (Fig. 5 C). D466C maintains a strong and fast C-type inactivation and K$^+$ selectivity, similar to those of the WT channel (Fig. 5 D).

*D501C in the intracellular half of S3 domain.* D501C currents are small when recorded under the same conditions as used in the other mutant channels ($[K]_o = 2$ mM). Increasing the amount of D501C cRNA injected also enhances the oocyte endogenous Cl$^-$ current (Fig. 6 A). Relative to the WT channel, the D501C activation curve is shifted in the depolarizing direction (Fig. 6 B). The rate of D501C activation is measured in 98 mM

$[K]_o$ (to boost the current amplitude). The envelope tests on the WT channel is also done in 98 mM $[K]_o$ for comparison. Fig. 6 C shows that the $\tau_o$ of D501C activation is shorter than that of WT in the $V_t$ range $<40$ mV, but the two datasets crossover with each other at 40 mV. Linear regression analysis gives an estimate of $K_o(0)$ and $z_a$ of 0.81 s$^{-1}$ and 1.0 for WT, and 2.28 s$^{-1}$ and 0.16 for D501C. Therefore, the D501C mutation markedly reduces the voltage sensitivity of the opening transition, although the rate constant of opening transition at 0 mV is higher than that of WT. Fig. 6 E shows D501C deactivation rate measured in 2 mM $[K]_o$. It is much faster than that of the WT channel. Because of the interference of oocyte Cl$^-$ current, leak-subtraction cannot be used in the construction of the $I_{f-a}$-V relationship for D501C (Fig. 6 D). The resulting $I_{f-a}$-V curve shows a plateau phase in the $V_r$ range of $-40$ to $+30$ mV. Since the I-V relationship of oocyte endogenous currents may have a positive slope in this voltage range, we suggest that D501C has at least some residual C-type inactivation, that offsets the positive slope of oocyte endogenous currents and creates the plateau phase. The apparent $E_{rev}$ suggested by the $I_{f-a}$-V relationship of D501C is slightly less negative than that of WT ($-90$ mV, Fig. 6 D). Again, this can be explained by the interference of
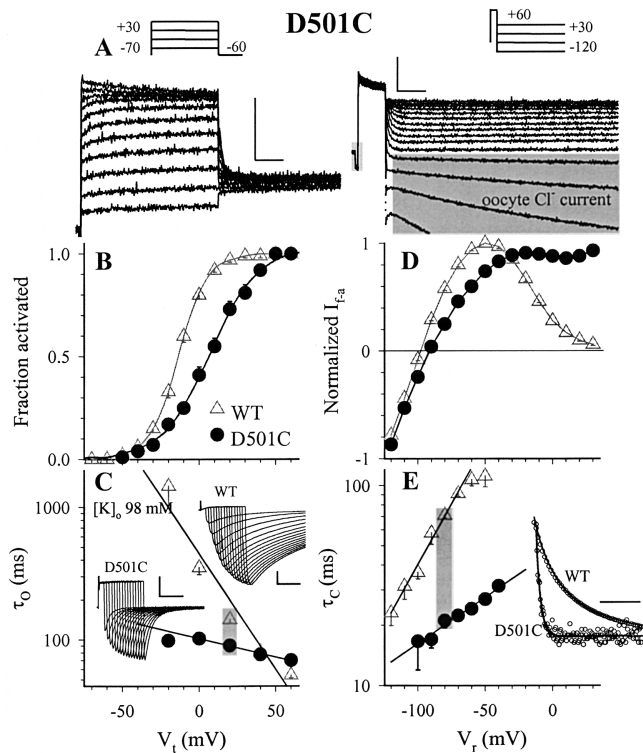
**FIGURE 6.** D501C channel function. The format is the same as that of Fig. 3. Note that in oocytes forced to overexpress D501C, the native Cl⁻ current becomes prominent (highlighted by gray shades in A). (B) D501C activation curve has $V_{0.5} = 7.6 \pm 2.5$ mV and $z_g = 1.66 \pm 0.09$. (C) Values of $\tau_o$ for both WT and D501C measured in 98 mM $[K]_o$. The data points are superimposed on lines calculated from Eq. 4, with $z_o$ values of 1.0 and 0.16 for WT and D501C, respectively. The D501C data in main graphs are averaged from four to seven cells each. Calibration bars correspond to 1 μA and 0.2 s.

oocyte endogenous currents. We conclude that D501C retains a high K⁺ selectivity.

Because of the uncertainties in characterizing D501C due to the small current amplitudes in 2 mM $[K]_o$ and the interference from oocyte Cl⁻ current, we further test the channel behavior in 98 mM $[K]_o$. Elevating $[K]_o$ greatly increases the current amplitude and reduces the interference from oocyte endogenous Cl⁻ current. Fig. 7 compares D501C data with WT data obtained in 98 mM $[K]_o$. The activation curve of D501C is shifted in the positive direction (Fig. 7 A), and the rate of deactivation is faster than that of WT (Fig. 7 B). These changes in the gating behavior of D501C confirm those reported in Fig. 6.

Similar to the observations with D466C (Fig. 5), the D501C mutation causes a decrease in the voltage-sensitivity of the activation gating process. Therefore, the $z_g$ value is reduced from 2.70 to 1.66 (measured in 2 mM $[K]_o$, Fig. 6 B), and from 2.79 to 1.45 when measured in 98 mM $[K]_o$ (Fig. 7 A). As mentioned above, the $z_a$ value is reduced from 1.0 to 0.16 (Fig. 6 C).
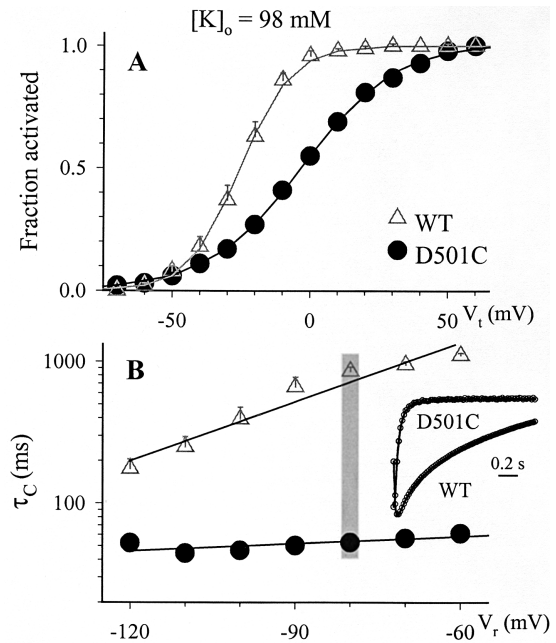


**FIGURE 7.** Comparison of gating behavior between D501C and WT recorded in 98 mM $[K]_o$. (A) Activation curves. For WT, $V_{0.5} = -25.4 \pm 2.2$ mV, $z_g = 2.79 \pm 0.03$. For D501C, $V_{0.5} = -2.8 \pm 0.6$ mV, $z_g = 1.45 \pm 0.05$. (B) Comparison of $\tau_c$ values between D501C and WT. (Inset) WT and D501C tail currents and curve fitting at $-80$ mV. Data are summarized from three to four cells each. Calibration bars correspond to 1 μA and 0.2 s.

*D509C in the extracellular half of S3 domain.* Relative to the WT channel, the D509C activation curve is shifted in the positive direction in a parallel fashion (Fig. 8 B). The rate of D509C activation is much slower than that of WT, but the voltage sensitivity remains the same (Fig. 8 C). D509C maintains a strong and fast C-type inactivation process and K⁺ selectivity (Fig. 8 D). Finally, the rate of D509C deactivation is faster than that of WT (Fig. 8 E). These changes in the channel gating behavior induced by the D509C mutation are similar to those described for D460C (Fig. 4).

*Accessibility of Introduced Thiol Side Chains to Extracellular MTS*

To further probe the structure-function relationship of HERG involving these aspartate residues, we test the accessibility of the introduced cysteine side chains to extracellular MTS reagents. An important assumption here is that the accessibility of thiol side chains in the cysteine-substituted mutants reflects the accessibility of the native side chains in the WT channel, i.e., cysteine substitution does not grossly perturb the channel conformation. Although the mutations all visibly alter the voltage dependence and kinetics of channel gating, conformational changes responsible for these alterations in gating are likely to be subtle. First, all mutants
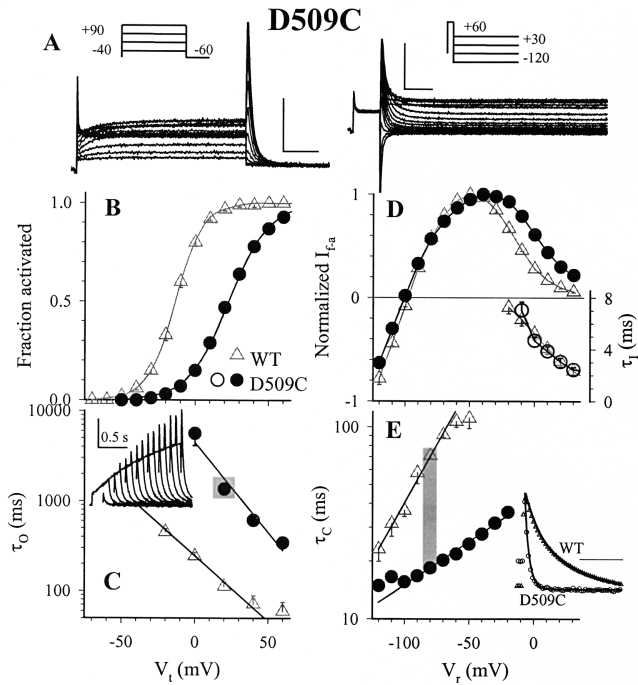
FIGURE 8. D509C channel function. The format is the same as that of Fig. 3. In B, the D509C activation curve has $V_{0.5} = 22.7 \pm 1.4$ mV and $z_g = 1.88 \pm 0.04$. In C, the D509C data points are superimposed on a line calculated from Eq. 4, with $z_o = 1.15$. The D509C data in main graphs are averaged from 9 to 10 cells each. Calibration bars correspond to 1 $\mu$A and 0.2 s (except panel C, for which the time calibration bar is 0.5 s).
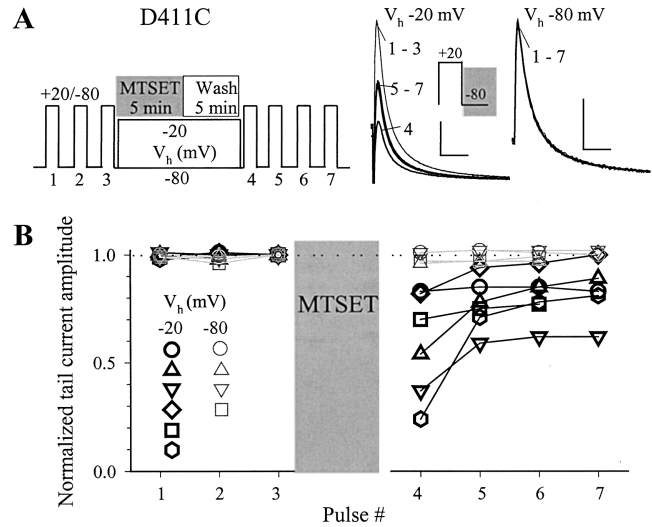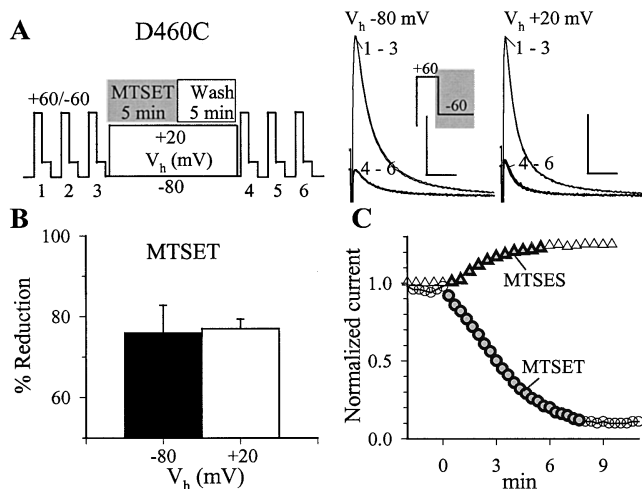
FIGURE 9. Testing the accessibility of thiol side chain at position 411 to extracellular MTSET. (A) Left, experimental protocol. Right, superimposed tail current traces (at −80 mV, gray shade in inset) recorded from two experiments. The $V_h$ and pulse numbers are marked. (B) Summary data. The peak amplitudes of tail currents are normalized by the control value just before MTSET application, and plotted against pulse numbers. Data points from different experiments are denoted by different symbols as denoted in the inset ($n = 6$ for $V_h$ −20 mV, and $n = 4$ for $V_h$ −80 mV). Calibration bars correspond to 1 $\mu$A and 0.1 s.

retain a high $K^+$ selectivity and the C-type inactivation process, indicating an intact outer mouth and pore function, as well as a proper communication between the voltage-sensing domain and the pore domains (which is essential for the C-type inactivation process; Gandhi et al., 2000; Liu et al., 2002). Second, mutation-induced changes in the free energy involved in the gating processes are small (calculated based on the shift of the activation curve). They amount to 1–3 kcal/mol, about the energy of one or two H-bonds in aqueous environment. Therefore, the mutant channels are sufficiently similar to the WT channel to justify the assumption stated above. In some cases, we test the effects of both MTSET and MTSES. Both reagents can increase the side chain volume of a modified cysteine. However, MTSET adds a positive charge while MTSES adds a negative charge to the side chain. Therefore, the resulting changes in channel function may yield some information about the underlying mechanism: a steric effect (similar between MTSET and MTSES) or a charge effect (different between the two). WT-HERG has 12 native cysteines, 5 of them are potentially accessible to external MTS (C445 and C449 in the extracellular S1-S2 linker, C555 and C566 in the S5 domain, and C643 in

the S6 domain). However, external MTSET or MTSES has no effects on WT-HERG, indicating that the native cysteines are either not accessible to extracellular MTS reagents, or modification of them by MTS has no impact on channel function (Liu et al., 2002). Thus, the observed effects on cysteine-substituted HERG mutants are likely due to MTS modification of the introduced cysteine side chains.

*411C is accessible to MTSET in a voltage-dependent manner.* Data for D411C are shown in Fig. 9. MTSET (1 mM) is applied for 5 min when the membrane voltage is held at −80 mV (most channels in the closed state) or −20 mV (channels in activated or inactivated state). MTSET is washed out for 5 min, and the effect on D411C current amplitude is evaluated. MTSET reduces the D411C current amplitude, and the effect can be seen only when it is applied during sustained depolarization at $V_h$ −20 mV, but not at $V_h$ −80 mV. However, once the $V_h$ is returned to −80 mV (when D411C channels are allowed to close), the MTSET effect gradually disappears. Thus, MTSET modification of 411C is voltage-dependent and unstable.
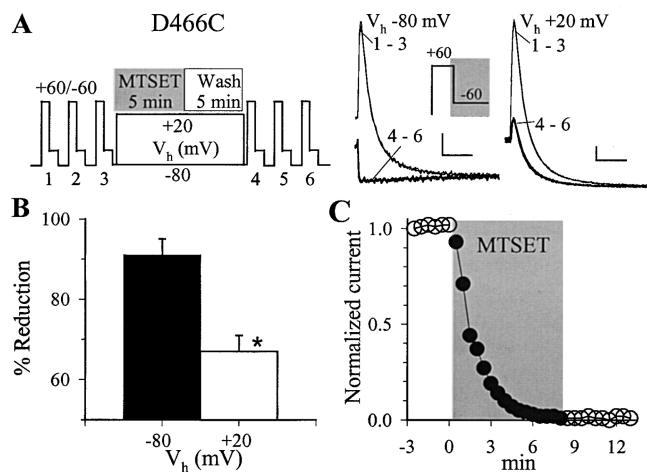
*Thiol side chain accessibility along the S2 domain (460C and 466C).* Thiol side chain at position 460 is accessible to extracellular MTSET applied either in closed state ($V_h$ −80 mV) or in activated/inactivated state ($V_h$ +20 mV) (Fig. 10). MATSET causes a 75 ± 3% reduc-

FIGURE 10. Testing the accessibility of thiol side chain at position 460 to extracellular MTSET or MTSES. The format of A is the same as that in Fig. 9 A. The voltage clamp protocol is modified because of the positive shift in D460C activation relative to D411C. (B) MTSET effects on D460C are similar when applied at either $V_h$ −80 or +20 mV ($n$ = 3 each). Data are taken from experiments similar to those shown in A. The MTSET effect is shown as a percentage of reduction, based on peak tail current amplitude of pulses 1 and 6. (C) Modification of 460C by MTSET reduces current amplitude while modification by MTSES has the opposite effect. Shown are time courses of changes in D460C tail current amplitude before, during and after exposure to MTSET (1 mM) or MTSES (10 mM). Data points during MTS exposure are highlighted. Similar findings are obtained in 15 (MTSET) and 6 (MTSES) cells. Calibration bars correspond to 1 μA and 0.1 s.

FIGURE 11. Testing the accessibility of thiol side chain at position 466 to extracellular MTSET. The format is similar to that of Fig. 10. Data in B are summarized from three cells each (*, P < 0.01). Calibration bars correspond to 0.5 μA and 0.1 s.

tion in D460C current amplitude ($n$ = 15). MTSES modification causes a modest increase (by 27 ± 3%, $n$ = 6, Fig. 10 C), and prevents further modification by MTSET (unpublished data). Thus, the 460 side chain is in a relatively wide open crevice around the S2, while side chain charge can impact on current amplitude. Further down the S2 helix, thiol side chain at position 466 is still accessible to extracellular MTSET. However, MTSET modification of 466C is stronger when applied at $V_h$ −80 mV (channels in the closed state) than at $V_h$ +20 mV (channels in activated/inactivated state) (Fig. 11, A and B). Furthermore, the suppressing effect of MTSET on D466C (>90% reduction) is stronger than that on D460C (Fig. 11 C vs. Fig. 10 C). Thus, the water-filled crevice around S2 narrows around 466.

*Thiol side chain accessibility along the S3 domain (509C and 501C).* MTSET modification of 509C causes little changes in the current amplitude, but there is a marked acceleration of channel deactivation (Fig. 12 A). The thiol group at position 509 are accessible to extracellular MTSET at either $V_h$ −80 mV (closed state) or $V_h$ 20 mV (activated/inactivated state) (Fig. 12 B). MTSES (10 mM) slows the deactivation rate of D509C, with little effects on the current amplitude (Fig. 12 C).

These findings indicate that 509 is in a wide open space where side chain charge has a great impact on the channel deactivation rate.

MTSET (1 mM) does not have consistent effects on D501C (monitored either by pulsing from $V_h$ −80 mV to 20 mV for 1 s once every 20 or 30 s for 5 min, $n$ = 24, or after a 5-min exposure during which the $V_h$ is held at −20 or 20 mV, $n$ = 2 each). Therefore, we conclude that thiol side chain at 501 is not accessible to the extracellular MTSET.

The above data show that cysteine-substitutions of aspartate residues in S1–S3 of HERG have distinct effects on the voltage dependence and kinetics of channel activation and deactivation, suggesting that these negative charges are importantly involved in the channel's gating processes. Furthermore, except position 501 thiol side chains introduced into the other positions are accessible to extracellular hydrophilic MTS reagents (in a voltage-dependent manner at some locations), suggesting that the original aspartates in WT HERG are potential targets for protonation by extracellular $H^+$ or binding by extracellular divalent cations. Although some side chains may not be quite accessible to the MTSET molecule (size > 6 A) (e.g., thiol side chain at 411), they may be readily accessible to the much smaller $H^+$ or $Ca^{2+}$ ions (ionic radius < 1 A). This may even apply to D501. Therefore, we next study whether and how these cysteine-substituted mutants can affect $H^+$ and $Ca^{2+}$ modulation of HERG.

*Effects of Extracellular $H^+$ on HERG: Role of Protonating Aspartate Residues in the Transmembrane Domains*

As shown previously, the most prominent effect of changing $pH_o$ on HERG is the alteration of deactiva-
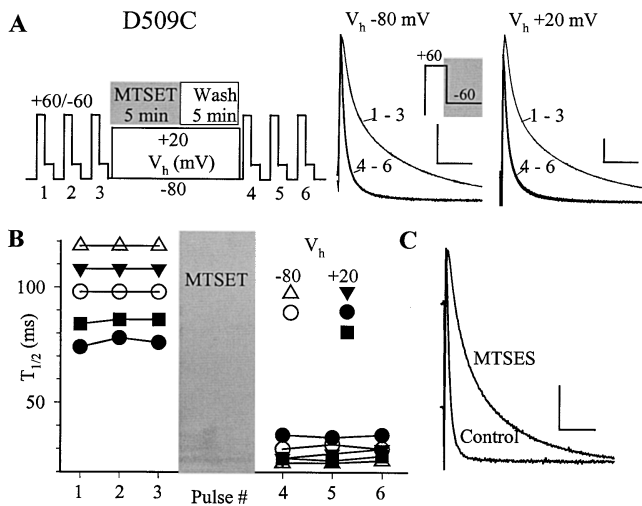
FIGURE 12. Testing the accessibility of thiol side chain at position 509 to extracellular MTSET or MTSES. The format of A and B is similar to that of Fig. 9, A and B. MTSET exposure induces a marked acceleration of D509C deactivation with little or no effects on the peak tail current amplitude. Therefore, the half-time of decay of tail current at $-60$ mV ($T_{1/2}$) is used as a measure of MTSET effect. Data in B are from five experiments denoted by different symbols. (C) MTSES (10 mM) slows D509C deactivation. Similar data are obtained from a total of three oocytes. Calibration bars correspond to 1 $\mu$A and 0.2 s.



FIGURE 13. Effects of changing pH$_o$ on the deactivation kinetics at $-60$ mV for WT and mutant channels. Each panel depicts tail current traces elicited by the protocol shown on top, recorded from the same cell at pH$_o$ 6.5 (long dashed line), 7.5 (thin solid line), and 8.5 (dotted line). The traces are scaled to match the peaks. Note differences in the time calibration bars (corresponding to 0.1 s). Similar data are obtained from a total of 4–6 oocytes each.

tion rate (Jiang et al., 1999). This is illustrated in Fig. 13, top left. For WT-HERG, changing pH$_o$ from 7.5 to 6.5 markedly accelerates deactivation, whereas changing pH$_o$ from 7.5 to 8.5 has the opposite (although more modest) effect. These effects are greatly reduced in D411C, and totally abolished in the other four mutants (Fig. 13). Similar findings are obtained in four to six cells each. These data are consistent with the notion that these aspartate residues are critically involved in pH$_o$ modulation of the deactivation rate in HERG. However, removing any one of them, leaving the other four still negatively charged, greatly attenuates or abolishes the pH$_o$ effect, as if all five negative charges are required for the manifestation of the pH$_o$ effect.

During these experiments, we also notice that D411C has a unique response to changing pH$_o$. As shown in Fig. 14, top, changing pH$_o$ in the range of 6.5 to 8.5 has little effect on the voltage dependence of activation in the WT channel. On the other hand, although changing pH$_o$ from 7.5 to 8.5 has little effect on the activation curve of D411C, changing pH$_o$ from 7.5 to 6.5 causes a marked positive shift. This shift seems to be selective for the Boltzmann component in the negative voltage range, such that the activation curve of D411C in pH$_o$ 6.5 can be well described by a single Boltzmann function. The activation curve of D411C is almost superimposable with the activation curve of WT-HERG at
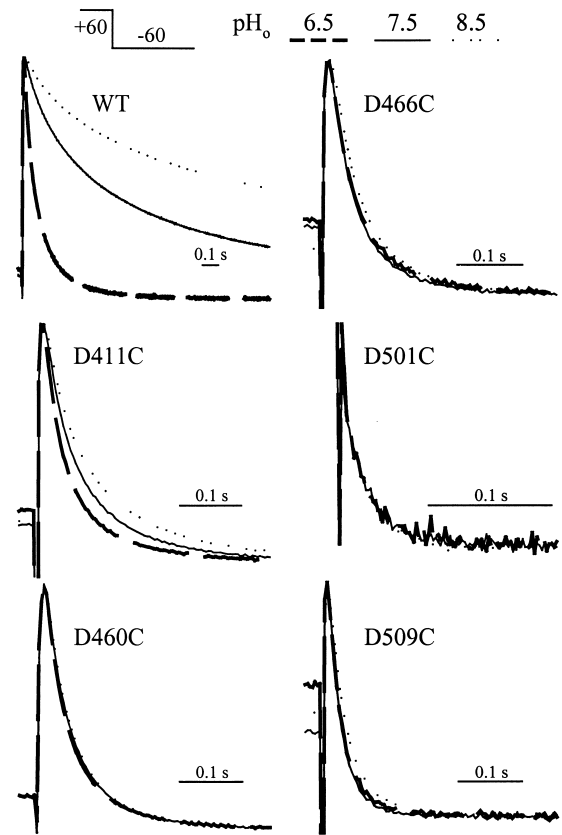
pH$_o$ 6.5. The implications of these findings, and those shown in Fig. 13, will be addressed in the DISCUSSION.

### Does D460 Contribute to a Metal Ion Binding Site in HERG?

The effects of elevating [Mg]$_o$ on HERG are essentially the same as those of elevating [Ca]$_o$ (Ho et al., 1998). We choose to study the effects of Ca$^{2+}$, instead of Mg$^{2+}$, because the mechanism of Ca$^{2+}$ action on HERG has been more thoroughly studied (Johnson et al., 1999, 2001). Fig. 15 shows that for WT-HERG, elevating [Ca]$_o$ from 1.8 to 10 mM causes a prominent positive shift in the activation curve (Fig. 15 B), and an acceleration of deactivation (Fig. 15 A, left, and C). Elevating [Ca$^{2+}$]$_o$ also causes a modest slowing of activation and a biphasic change in the current amplitude (Fig. 15 A, left, the test pulse current is increased at the end of the depolarization step, but the peak amplitude of the following tail current is reduced). In EAG, D278 is an important contributor to the Mg$^{2+}$ binding site (Silverman et al., 2000). Neutralizing D278 totally abolishes the slowing
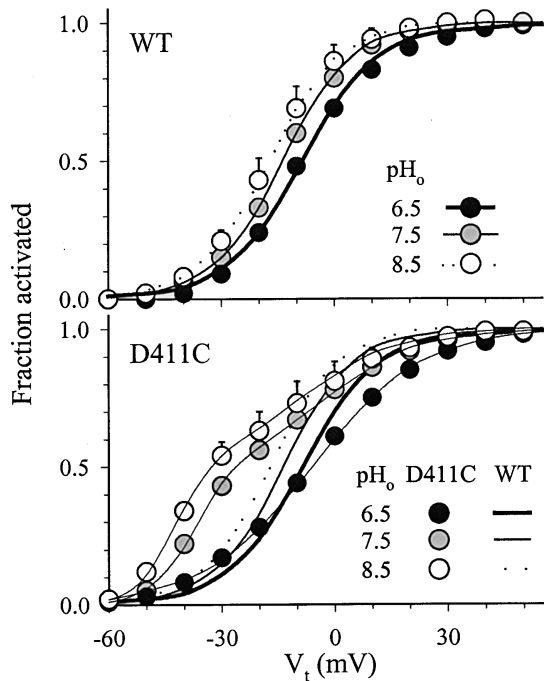
FIGURE 14. Effects of changing $pH_o$ on the voltage dependence of activation for WT (top) and D411C (bottom). The voltage clamp protocol and data analysis are the same as those described for Figs. 2 A and 3 A, respectively, except D411C data at $pH_o$ 6.5 (fit with a single, but not double, Boltzmann function). Data points at $pH_o$ 6.5, 7.5, and 8.5 are shown as black, gray, and white circles, respectively, and superimposed on curves calculated from the Boltzmann functions. For comparison, the WT activation curves are shown again in the bottom panel. Data are summarized from 4–6 cells each.

effect of $Mg^{2+}$ on EAG activation. On the other hand, neutralizing the 'D278-equivalent' in HERG (D460C) does not alter the effects of $Ca^{2+}$ on HERG channel function, including the positive shift in the activation curve (Fig. 15 B), acceleration of deactivation (Fig. 15 A, right, and C), and the biphasic change in the current amplitude (Fig. 15 A, right). Therefore, D460 in HERG and D278 in EAG are not functionally equivalent.

DISCUSSION

Cysteine substitutions of the aspartate residues in S1–S3 of HERG have distinct effects on the channel function. The phenotypes of the 5 mutants studied here (D411C, D460C, D466C, D501C, and D509C) can be summarized as the following. First, there are three patterns of changes in the voltage dependence of activation. For D411C in the S1 domain, 50% of the channels are activated in a more negative voltage range than the WT channel, and the rate of activation is markedly accelerated. For D460C and D509C in the extracellular half of S2 and S3, respectively, the activation curve is shifted in the positive direction and the rate of activation is slowed, but there is little change in the voltage dependence of the activation gating process. For D466C and D501C that are in the intracellular half of S2 and S3, the activation curve is shifted in the positive direction. Furthermore, there is a marked reduction of voltage sensitivity in the activation-gating process. Second, all the mutant channels manifest an accelerated deactivation process. In contrast to the marked changes in the activation and deactivation processes, all the mutants retain the ability to C-type inactivate and to select for $K^+$ ions as the charge carrier, indicating that the pore-domain function and the communication between the pore-domain and the voltage-sensing domain are maintained.

*Role of Transmembrane Domain Aspartate Residues in the Activation Process of HERG*

Two aspects of the activation process are characterized: activation curve and rate of activation. Two parameters are generated from fitting the activation curve with the Boltzmann function: $V_{0.5}$ (half-maximum activation voltage) and $z_g$ (apparent gating charge for channel activation). The ideal way to measure the gating charge is to record gating currents (Bezanilla, 2000). However, due to the slow rate of HERG activation, recording gating currents from the HERG channel is difficult (Smith and Yellen, 2002). Therefore, although $z_g$ most likely underestimates the number of gating charges involved in HERG activation (Bezanilla, 2000), it nevertheless helps us compare the mutant channels in their voltage sensitivity of activation. A concern is whether changes in the position or steepness of the activation curve seen in the mutant channels may have contribution from mutation-induced alterations in the inactivation process, because some of the channels may not have recovered from inactivation at the peak of the tail current. Although we cannot absolutely exclude this possibility, we believe this contribution is not significant. We show that the rate of inactivation is not altered by the mutations, suggesting that the inactivation process is little affected.

The time course of activation of WT and mutant channels can be well described by a single exponential function with a time delay. Two parameters are obtained by a linear regression of the relationship between $\ln(1/\tau_o(V))$ and $V_t$: $K_o(0)$ (rate constant of opening transition at 0 mV) and $z_a$ (gating charge involved in channel opening). Mutation-induced changes in the $K_o(0)$ value will indicate how the mutation affects the activation energy involved in the transition from the last closed state ($C_n$ in Scheme I) to a transition state, and changes in $z_a$ will reveal whether the amount of gating charge involved in this transition is altered.

*D466 and D501 may be directly involved in voltage sensing during HERG activation.* For both D466C and D501C,
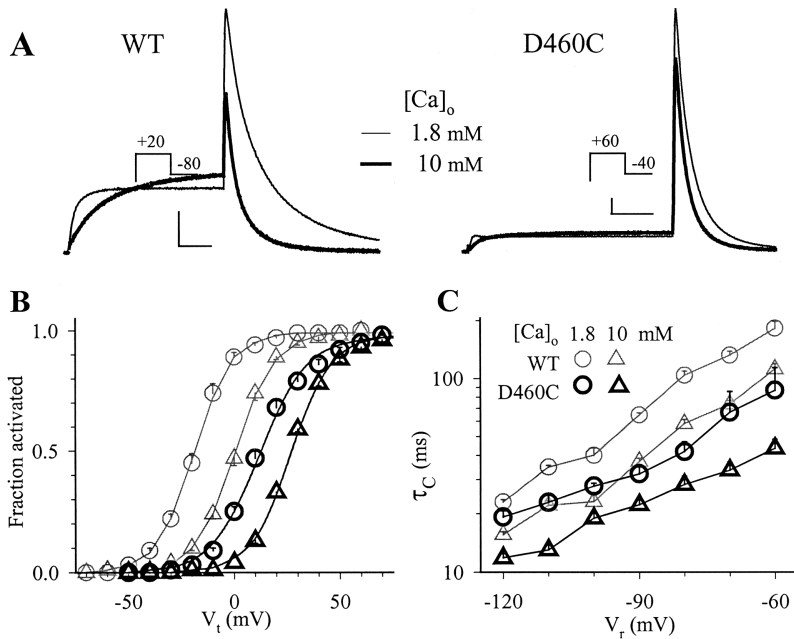
FIGURE 15. Elevating $[Ca]_o$ has similar effects on WT and D460C. (A) Original current traces of WT and D460C from same cells in specified $[Ca]_o$ (1.8 mM thin traces, 10 mM thick traces), elicited by the voltage clamp protocols diagrammed in respective insets. (B) Voltage dependence of WT and D460C activation measured in 1.8 or 10 mM $[Ca]_o$. (C) Time constant of fast component of deactivation for WT and D460C measured in 1.8 and 10 mM $[Ca]_o$. The symbols shown in inset of C also apply to B. Data points in B and C are summarized for four cells each. Calibration bars correspond to 1 μA and 0.2 s.

the $z_g$ value from the Boltzmann fit is reduced. Importantly, the $z_a$ value is markedly reduced, although the $K_o(0)$ value is not altered (in D466C, Fig. 5 C) or even increased (in D501C, Fig. 6 C). Therefore, removing the negative charge at either 466 or 501 reduces the amount of gating charge involved in channel opening, suggesting that in the WT channel aspartates at these two locations deep in the cytoplasmic half of S2 and S3 may contribute to voltage sensing during activation. This may occur through a state-dependent interaction between D466 and/or D501 with a positive charge in the S4, or from a movement of the negative charge(s) relative to the membrane electrical field during gating. For D466, either scenario is consistent with results from the accessibility test: the thiol side chain at 466 is accessible to extracellular MTSET preferentially in the closed state. It has been suggested that the "D466-equivalent" in the Shaker channel, E293, directly contributes to the channel's gating charge because removing the negative charge at 293 can reduce the number of gating charges by ~50% (Seoh et al., 1996).

*D460 and D509 increase the stability of HERG in the activated state relative to the closed state.* D460C and D509C manifest similar changes in the activation gating process: a parallel shift of the activation curve in the positive direction, and a slowing of channel opening without alteration in the voltage sensitivity (reduction in $K_o(0)$, without change in $z_a$). These suggest that cysteine substitution of either aspartate increases the activation energy involved in the transition from the closed state to the transition state during activation, but the amount of gating charge involved in channel activation remains the same. The accessibility tests indicate that

thiol side chains at both positions are in a relatively wide open space, accessible to extracellular MTS reagents at both $V_h$ −80 mV (channels in the closed state) and +20 mV (channels in activated/inactivated state). This is consistent with the opposite effects of MTSET and MTSES on the two mutants. MTSET modification of 460C decreases the current amplitude, whereas MTSES modification causes a modest increase. MTSET modification of 509C accelerates the rate of channel deactivation, whereas MTSES modification has the opposite effect, and neither alters the 509C current amplitude. Therefore, the effects of MTS modification at both locations are due to the added charge, but not due to the added side chain volume. The mechanism by which D460 and D509 influence the channel's activated gating process is not clear.

*D411 in the S1 domain stabilizes HERG in the closed state.* The D411C mutation shifts the voltage dependence of activation in the negative direction and accelerates the rate of channel opening. These observations can be explained by proposing that the negative charge at position 411 can pair with a nearby positive charge when the WT channel is in the closed state. Membrane depolarization induces conformational changes in the S1 domain, or in its relation to the surroundings. These changes need to disrupt the ion pairing before the channel can reach the open state. Therefore, removing the negative charge at 411 can destabilize the channel in the closed state relative to the transition state during activation. This scenario is consistent with two other observations reported here. First, changing $pH_o$ from 7.5 to 6.5 shifts the activation curves of WT and D411C channels so that they superimpose at $pH_o$ 6.5. This in-

crease in [H$^+$] may protonate the aspartate side chain at 411, abolishing its stabilizing effect on the closed state and negating the difference between WT and D411C. A corollary of this inference is that in WT-HERG changing pH$_o$ from 7.5 to 6.5 may favor channel opening by protonating D411. This will offset the positive shift in the voltage dependence of channel activation associated with proton effect on the external surface potential. The dual effect of extracellular protons on HERG gating may explain why changing pH$_o$ from 7.5 to 6.5 has such a small effect on V$_{0.5}$ of HERG activation (positive shift by $\sim$5 mV, Fig. 14), whereas a similar change in pH$_o$ can cause a much larger effect on other voltage-gated channels (e.g., V$_{0.5}$ positive shift by $\sim$25 mV in Kv1.5; Zhang et al., 2003). Second, the thiol side chain at 411 is accessible to extracellular MTSET when the membrane voltage is held at $-20$ mV (channels in activated/inactivated states), but not at $-80$ mV (channels in the closed state). This state dependence of accessibility indicates that during the activation process, there are conformational changes in S1 or in its surroundings at the level of 411, and these changes may cause the 411 side chain to switch from pairing with a nearby residue (not reactive to MTSET) to facing a water-filled crevice (reactive to MTSET).

### How Are the Aspartate Residues Involved in the Deactivation Process of HERG?

The deactivation process in the HERG channel is much more complex than a simple reversal of the S4 movement. In WT-HERG, the deactivation rate is a function of the voltage and duration of the previous depolarization pulse (Viloria et al., 2000). This can be explained by a time-dependent interaction between the NH$_2$-terminal PAS domain and the gating machinery, likely the S4-S5 linker (Wang et al., 1998; Viloria et al., 2000). Upon membrane depolarization, the PAS domain can bind to the S4-S5 linker only when the channel reaches the open state. Upon repolarization, the channel cannot close until the PAS domain has dissociated from the S4-S5 linker. Therefore, the deactivation rate will be slower after a stronger or a longer depolarization pulse (more PAS binding to the S4-S5 linker), until the channels are fully activated (maximal PAS binding).

All five mutants accelerate the deactivation rate. Do these five aspartate residues contribute to the deactivation process in an additive manner (e.g., each making an independent contribution to the stability of the WT channel in the open state), or in a concerted manner (e.g., all five working together to stabilize the WT channel in the open state)? We can get some clues from the pH$_o$ experiments: neutralizing any one of these negative charges, leaving the other four intact, can largely prevent the pH$_o$ effects on the deactivation process. We propose that there may be a "master-switch" in the

HERG channel that keeps the deactivation rate slow. Turning off this switch will set in motion a fast deactivation process. All five aspartates need to be present simultaneously to prevent the master-switch from turning off. What domain(s) may constitute this master-switch? The interaction between the PAS domain and the S4-S5 linker is a good candidate. This is consistent with our previous observation that deleting a large part of the NH$_2$-terminal region from the HERG channel, including the PAS domain, creates a phenotype similar to that of the mutants reported here: the deactivation rate is markedly accelerated and the response of deactivation rate to changes in pH$_o$ is markedly reduced (Jiang et al., 1999).

### Is There a Metal Ion Binding Site in the Transmembrane Domains of HERG?

It has been shown that $-3$ in S2 (D278) and $-6$ in S3 (D327) together form a metal ion binding site in the transmembrane domain of the EAG channel, and Mg$^{2+}$ slows EAG activation by binding to this site (Silverman et al., 2000; Papazian et al., 2002; Schonherr et al., 2002). Can this be generalized to HERG? Although the effects of Mg$^{2+}$ on HERG are different from those on EAG, this may result from the intrinsic differences in the gating behavior between the two channels, but not due to a difference in mechanism. A more direct test is to neutralize the "D278-equivalent" in the HERG channel (D460). If this aspartate contributes to a metal ion binding site in HERG, as in the EAG channel, then removing the negative charge should abolish the effects of Mg$^{2+}$ or Ca$^{2+}$ (which affects HERG in the same fashion, and likely by the same mechanism) on HERG.

Our data show that D460C does not alter the effects of Ca$^{2+}$ on HERG. Therefore, there is no evidence for a metal ion binding site in the HERG channel, equivalent to that described for the EAG channels. The effects of Mg$^{2+}$ and Ca$^{2+}$ on the HERG channel can be explained by one or a combination of the following mechanisms. First, extracellular divalent cations can bind to negative surface charges on the HERG protein and alter the membrane electrical field sensed by S4 (Johnson et al., 1999). E518 and E519 in the extracellular S3-S4 linker may constitute the external divalent cation binding site in HERG (Johnson et al., 2001). Second, extracellular divalent cations can enter and block the HERG pore in a voltage- and time-dependent fashion (Ho et al., 1998). This can better explain the biphasic effect of Ca$^{2+}$ on the current amplitude: Ca$^{2+}$ decreases the peak tail current amplitude by blocking the pore at negative voltages. It unblocks at positive voltages, but at the same time interferes with the C-type inactivation process, thus causing an increase in the test pulse current amplitude late during depolarization.
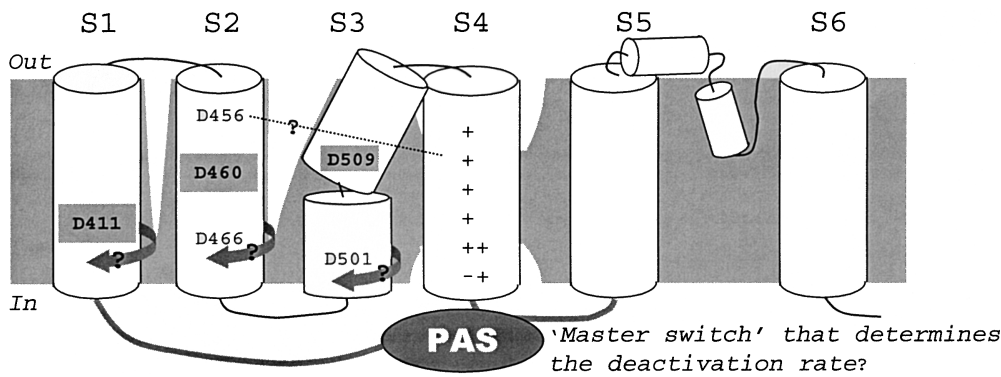
FIGURE 16. Cartoon of a HERG subunit highlighting conclusions from this study: (a) the penetration of water-filled crevices around S1 and S2 deduced from the accessibility data, and (b) an apparent lack of a metal ion binding site formed by D460 and D509 in HERG as that described for EAG. This cartoon also highlights the following proposals (indicated by ?): (a) D466 and D501 may contribute to gating charge by moving relative to the membrane electrical field either due to a rotation of S2 and/or S3, or due to changes in the crevice around them. (b) There may be a rotation of S1, or the surrounding crevice, at the level of D411. (c) D456 may form an ion pair with S4's positive charge. And (d) binding of the $NH_2$-terminal PAS domain to the cytoplasmic S4-S5 linker serves as a "master-switch" that controls the rate of channel deactivation.

## Structural Implications of our Findings

Fig. 16 summarizes what we can conclude (and propose) from our findings. (a) Our data suggest that water-filled crevices penetrate deep into the HERG protein core, reaching the level of 411 around S1 and the level of 466 around S2. (b) Accessibility of side chains at these two positions to extracellular aqueous phase is voltage dependent: 411 side chain is accessible at $V_h$ −20 mV, whereas 466 side chain is accessible preferably at $V_h$ −80 mV. Therefore, during alterations in the membrane potential, conformational changes occur in S1 and S2, or in the crevices around them. (c) Side chains at 460 and 509 are in a relatively wide open space readily accessible to the extracellular aqueous phase. A kink in the S3 domain, caused by the proline at position 507 (Fig. 1) (Li-Smerin and Swartz, 2001), may help create this wide crevice between S2 and S3. (d) D411 may form an ion pair with a nearby positive charge when the HERG channel is in the closed state. (e) D466 and D501 are intimately involved in the voltage-sensing machinery in HERG. Given the possibility that the S2 domain may be surrounded by water-filled crevices on a large portion of its surface and carries a modest density of negative charges along its length, it is not unlikely that S2 may move in response to a change in the membrane voltage and that D466 may be a direct contributor to the HERG channel's gating charge. (f) D456 may plays a critical role in channel protein folding and maturation, similar to the role of E283 in the Shaker channel. (g) To account for our data, we hypothesize that there is a "master-switch" in HERG that maintains a slow rate of deactivation. Turning off this master-switch will set the channel in a fast deactivation mode. To keep the master-switch in the ON position requires the simultaneous presence of all five aspartate residues (D411, D460, D466, D501, and D509). A candidate for this master-switch is the $NH_2$-terminal PAS domain.

REFERENCES

Bezanilla, F. 2000. The voltage sensor in voltage-dependent ion channels. *Physiol. Rev.* 80:555–592.

Cole, K.S., and J.W. Moore. 1960. Potassium ion current in the squid giant axon: dynamic characteristic. *Biophys. J.* 1:1–14.

Gandhi, C.S., and E.Y. Isacoff. 2002. Molecular models of voltage sensing. *J. Gen. Physiol.* 120:455–463.

Gandhi, C.S., E. Loots, and E.Y. Isacoff. 2000. Reconstructing voltage sensor-pore interaction from a fluorescence scan of a voltage-gated K+ channel. *Neuron.* 27:585–595.

Herzberg, I.M., M.C. Trudeau, and G.A. Robertson. 1998. Transfer of rapid inactivation and sensitivity to the class III antiarrhythmic drug E-4031 from HERG to M-eag channels. *J. Physiol.* 511:3–14.

Ho, W.-K., I. Kim, C.O. Lee, and Y.E. Earm. 1998. Voltage-dependent blockade of *HERG* expressed in *Xenopus* oocytes by external $Ca^{2+}$ and $Mg^{2+}$. *J. Physiol.* 507:631–638.

Islas, L.D., and F.J. Sigworth. 2001. Electrostatics and the gating pore of *Shaker* potassium channels. *J. Gen. Physiol.* 117:69–89.

Jiang, M., W. Dun, and G.-N. Tseng. 1999. Mechanism for the effects of extracellular acidification on *hERG* channel function. *Am. J. Physiol.* 277:H1283–H1292.

Johnson, J.P., J.R. Balser, and P.B. Bennett. 2001. A novel extracellular calcium sensing mechanism in voltage-gated potassium ion channels. *J. Neurosci.* 21:4143–4153.

Johnson, J.P., F.M. Mullins, and P.B. Bennett. 1999. Human *ether-a-go-go*-related gene K+ channel gating probed with extracellular $Ca^{2+}$. Evidence for two distinct voltage sensors. *J. Gen. Physiol.* 113:565–580.

Li-Smerin, Y., and K.J. Swartz. 2001. Helical structure of the COOH

terminus of S3 and its contribution to the gating modifier toxin receptor in voltage-gated ion channels. *J. Gen. Physiol.* 117:205–217.

Liu, J., M. Zhang, M. Jiang, and G.-N. Tseng. 2002. Structural and functional role of the extracellular S5-P linker in the HERG potassium channel. *J. Gen. Physiol.* 120:723–737.

Lu, Z., A.M. Klem, and Y. Ramu. 2002. Coupling between voltage sensors and activation gate in voltage-gated K$^+$ channels. *J. Gen. Physiol.* 120:663–676.

Morais Cabral, J.H., A. Lee, S.L. Cohen, B.T. Chait, M. Li, and R. MacKinnon. 1998. Crystal structure and functional analysis of the HERG potassium channel N-terminus: an eukaryotic PAS domain. *Cell.* 95:649–655.

Papazian, D.M., W.R. Silverman, M.-C.A. Lin, S.K. Tiwari-Woodruff, and C.-Y. Tang. 2002. Structural organization of the voltage sensor in voltage-dependent potassium channels. Novartis Foundation Symposium. 245:178–192.

Robertson, G.A., J.W. Warmke, and B. Ganetzky. 1996. Potassium currents expressed from *Drosophila* and mouse *eag* cDNAs in *Xenopus* oocytes. *Neuropharmacology.* 35:841–850.

Sanguinetti, M.C., C. Jiang, M.E. Curran, and M.T. Keating. 1995. A mechanistic link between an inherited and an acquired cardiac arrhythmia: HERG encodes the I$_{Kr}$ potassium channel. *Cell.* 81:299–307.

Schonherr, R., L.M. Mannuzzu, E.Y. Isacoff, and S.H. Heinemann. 2002. Conformational switch between slow and fast gating modes: allosteric regulation of voltage sensor mobility in the EAG K$^+$ channel. *Neuron.* 35:935–949.

Schreibmayer, W., H.A. Lester, and N. Dascal. 1994. Voltage clamping of *Xenopus laevis* oocytes utilizing agarose-cushion electrodes. *Pflugers Arch.* 426:453–458.

Seoh, S.-A., D. Sigg, D.M. Papazian, and F. Bezanilla. 1996. Voltage-sensing residues in the S2 and S4 segments of the *Shaker* K$^+$ channel. *Neuron.* 16:1159–1167.

Silverman, W.R., C.-Y. Tang, A.F. Mock, K.-B. Huh, and D.M. Papazian. 2000. Mg$^{2+}$ modulates voltage-dependent activation in Ether-a-go-go potassium channels by binding between transmembrane segments S2 and S3. *J. Gen. Physiol.* 116:663–677.

Smith, P.L., and G. Yellen. 2002. Fast and slow voltage sensor movements in HERG potassium channels. *J. Gen. Physiol.* 119:275–293.

Tang, C.-Y., F. Bezanilla, and D.M. Papazian. 2000. Extracellular Mg$^{2+}$ modulates slow gating transitions and the opening of *Drosophila* ether-a-go-go potassium channels. *J. Gen. Physiol.* 115:319–337.

Terlau, H., J. Ludwig, R. Steffan, O. Pongs, W. Stuhmer, and S.H. Heinemann. 1996. Extracellular Mg$^{2+}$ regulates activation of rat eag potassium channel. *Pflugers Arch.* 432:301–312.

Tiwari-Woodruff, S.K., M.-C.A. Lin, C.T. Schulteis, and D.M. Papazian. 2000. Voltage-dependent structural interactions in the *Shaker* K$^+$ channel. *J. Gen. Physiol.* 115:123–138.

Tiwari-Woodruff, S.K., C.T. Schulteis, A.F. Mock, and D.M. Papazian. 1997. Electrostatic interactions between transmembrane segments mediate folding of shaker K$^+$ channel subunits. *Biophys. J.* 72:1489–1500.

Tristani-Firouzi, M., J. Chen, and M.C. Sanguinetti. 2002. Interactions between S4-S5 linker and S6 transmembrane domain modulate gating of HERG K$^+$ channels. *J. Biol. Chem.* 277:18994–19000.

Tseng-Crank, J.C.L., G.-N. Tseng, A. Schwartz, and M.A. Tanouye. 1990. Molecular cloning and functional expression of a potassium channel cDNA isolated from a rat cardiac library. *FEBS Lett.* 268:63–68.

Viloria, C.G., F. Barros, T. Giraldez, D. Gomez-Varela, and P. de la Pena. 2000. Differential effects of amino-terminal distal and proximal domains in the regulation of human *erg* K$^+$ channel gating. *Biophys. J.* 79:231–246.

Wang, J., M.C. Trudeau, A.M. Zappia, and G.A. Robertson. 1998. Regulation of deactivation by an amino terminal domain in *Human ether-a-go-go gene* potassium channels. *J. Gen. Physiol.* 112:637–647.

Warmke, J.W., and B. Ganetzky. 1994. A family of potassium channel genes related to eag in *Drosophila* and mammals. *Proc. Natl. Acad. Sci. USA.* 91:3438–3442.

Zhang, S., H.T. Kurata, S.J. Kehl, and D. Fedida. 2003. Rapid induction of P/C-type inactivation is the mechanism for acid-induced K$^+$ current inhibition. *J. Gen. Physiol.* 121:215–225.